

Slip-Mediated Dewetting of Polymer Microdroplets

Joshua D. McGraw^{1*}, Tak Shing Chan^{1,2}, Simon Maurer¹, Thomas Salez³,
Michael Benzaquen³, Élie Raphaël³, Martin Brinkmann^{1,2}, Karin Jacobs¹

July 14, 2015

Abstract

Classical models for wetting predict that an infinite work is required to move a three-phase contact line, defined as the line where a liquid-vapor interface intersects a solid surface. Assuming a slip boundary condition, in which the liquid slides against the solid, such an unphysical prediction is avoided. In this article, we present the results of experiments in which a contact line moves and where slip is a dominating and controllable factor. Spherical cap shaped polystyrene microdroplets, with non-equilibrium contact angle, are placed on solid self-assembled monolayer coatings from which they dewet. The relaxation is monitored using *in situ* atomic force microscopy, and the results are in agreement with scaling analysis and boundary element numerical integration of the governing Stokes equations, including a Navier slip boundary condition. We find that slip has a strong influence on the droplet evolutions, both on the transient non-spherical shapes and contact line dynamics.

Unexpected flow phenomena emerge when the size of a liquid system is reduced below a certain length scale, typically on the order of a few to hundreds of nanometers [1–3]. Approaching this scale, effects associated with interfaces become increasingly important. One such effect is slip, wherein fluid slides along a solid confining boundary. Examples include flow of single-component [4, 5] and complex fluids [6, 7] in micro- and nano-channels, as well as dewetting [8, 9] and interfacial instabilities [10] of molten polymer films. The present work demonstrates that the relaxation of micron-sized droplets in contact with a solid planar surface is strongly influenced by slip effects.

The no-slip boundary condition assumes no relative motion between liquid and solid at the phase boundary. This condition was historically assumed to be valid in all practical cases [3]. However, the no-slip condition is an empirical assumption and

recent experimental techniques [1–3] have reached nanometric resolution, allowing for a critical assessment of this hypothesis at microscopic length scales. Slip lengths – defined as the distance beyond the solid over which a linear extrapolation of the velocity field reaches zero [11] – on the order of tens of nanometers for small-molecule liquids [1–3, 12–15] and gases [16, 17], and up to a couple of hundred nanometers [18–20], are now commonly reported. In dewetting thin polymer films, where the molecules are larger and highly coupled to the bulk liquid [21–23], slip lengths up to tens of micrometers have been reported [9, 10, 24–29].

Given the existence of such boundary conditions, it is relevant to ask what effect slip might have on the motion of a three-phase contact line. On one hand, a no-slip boundary condition at the contact line leads to a non-integrable divergence of the stress, and thus implies that moving a contact line requires infinite work. On the other hand, in common experience we are surrounded by liquid interfaces moving along solid surfaces, from water droplets on a wind screen, to the displacement of air by liquid through a capillary or porous medium. This apparent paradox [30] of contact line

¹Experimental Physics, Saarland University, D-66041 Saarbrücken, Germany

²Max Planck Institute for Dynamics and Self-Organization (MPIDS), 37077 Göttingen, Germany

³PCT Lab, UMR Gulliver 7083, ESPCI Paristech, PSL Research University, Paris, France

*email: j.mcgraw@physik.uni-saarland.de

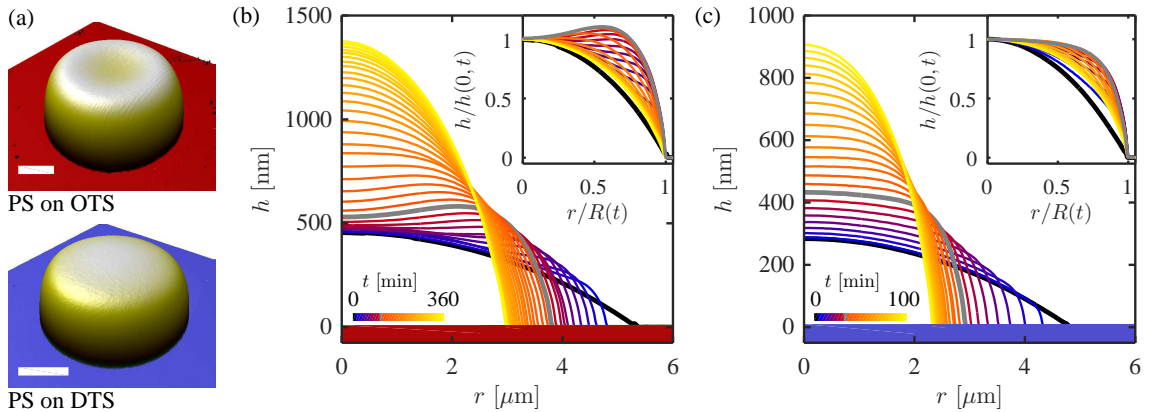


Figure 1: (a) Experimental atomic force microscopy data for PS microdroplets dewetting from OTS (top) and DTS (bottom) self-assembled monolayers; scale bars are $2\ \mu\text{m}$ and the height scales can be seen from the grey lines in (b) and (c). (b) Experimental height profile evolution of the PS droplet dewetting from OTS shown in (a). Time between lines is approximately 10 min. (c) Experimental height profile evolution of the PS droplet dewetting from DTS shown in (a). Time between lines is approximately 4 min. Insets show height profiles, with the radial coordinate r and height profile $h(r, t)$ scaled by the contact line radius $R(t)$ and central droplet height $h(0, t)$. Inset color schemes are as in the main figures.

motion (CLM) has attracted the attention of many researchers [21, 31–35] over at least the last four decades [30, 36].

Several models [3] have been proposed to allow for CLM, which may be broadly classified into i) molecular kinetic [32, 37, 38] and ii) hydrodynamic processes. The second of these may be further subdivided into models employing precursor films [21, 39–45], and slip [30, 36, 46–49]. These mechanisms share the feature of a length scale typically of nanometric range – often much smaller than the extension of liquid interfaces considered in the literature [38, 50–52]. When valid, this separation of length scales in the CLM problem allows for the assumption that dissipation is localized near the contact line, while the rest of the liquid-vapor interface is treated in a quasi-static approximation [34, 53, 54]. Following this idea, the details of the different mechanisms mentioned above are hidden inside a single length scale [21, 33], making it difficult to distinguish between them.

In this article, we present a study of dewetting polymer microdroplets, where the slip lengths involved are comparable to the typical droplet heights. The latter point allows us to formulate a single hydrodynamic description of the whole

system, avoiding difficulties associated with multi-scale modelling. The general result is that slip significantly influences the transient droplet profiles, which are non-spherical and thus not quasi-static (Fig. 1(a)). Furthermore, the velocity of the receding contact line is found to be orders of magnitude faster than the one expected for multi-scale systems [33, 34, 38, 50–52].

We use atomic force microscopy (AFM) to image dewetting polystyrene (PS) droplets with typical size of order $1\ \mu\text{m}$. As initial conditions, glassy spherical cap shaped droplets were prepared as in Ref. [44] resulting in initial contact angles $\theta_0 = 9 \pm 3^\circ$. The substrates were Si wafers pre-coated with self-assembled monolayers (SAMs) of octadecyl- or dodecyl-trichlorosilane (OTS and DTS). OTS and DTS are chemically similar, resulting in identical equilibrium Young-Dupré contact angles with PS, $\theta_\infty = 62 \pm 3^\circ$. Advantageously for this study, the physical structure of the SAMs is different leading to $b_{\text{DTS}}/b_{\text{OTS}} \approx 10$. The slip lengths were measured from independent experiments [29], wherein rim shape analysis [28, 55] of dewetting holes – using the same PS on the same substrates as used here – was performed. In that analysis, it was found that $b_{\text{OTS}} = 160 \pm 30\ \text{nm}$ and

$b_{\text{DTS}} = 1500 \pm 200$ nm. The reader is referred to the materials and methods section for more details on the sample preparation and experimentation.

Figs. 1(b) and (c) show full sequences of transient droplet profiles, $h(r, t)$, observed during the dewetting process on OTS and DTS covered substrates. The shapes highlighted in Fig. 1(a) were chosen such that the profiles deviate maximally from a spherical cap, as demonstrated in the insets (bold grey lines) of Figs. 1(b) and (c). For both substrates, the bold black line shows the initial shape, as prepared in the glassy state, with initial contact angle $\theta_0 \ll \theta_\infty$. When the temperature is increased to above the glass transition, we observe a flow (colored lines) that causes the contact line to move inwards, while volume conservation ensures that material is collected toward the center of the droplet. We stress here that the capillary number, $Ca \equiv \dot{R}\eta/\gamma$, of the early flow is of order ~ 1 for DTS, and ~ 0.1 for OTS, which are much larger than those often considered [33, 34, 38, 50–52]. In Ca , \dot{R} is the contact line velocity, γ is the PS-air surface tension and η is the PS viscosity (see materials and methods).

The PS droplet dewetting from OTS in Fig. 1(b) transiently forms a bump and for some time exhibits a positive curvature at the droplet center, $\partial_r^2 h|_{r=0} > 0$. Note that this qualitative feature was observed previously using numerical resolution of a 2D thin-film equation including a precursor film [42], and a qualitatively similar shape transition can be seen in dewetting polymer films with slip [9, 27]. In addition, the central droplet height does not change significantly until the width of the bump is comparable to the contact line radius, R . At late times, for both OTS and DTS, the curvature is always negative as the droplet relaxes to its final spherical-cap shape with the same contact angle θ_∞ . In contrast to the evolution on OTS, the PS droplet dewetting from DTS does not show a pronounced bump. Furthermore, at the earliest accessible experimental time (several minutes), the central droplet height is already increasing on DTS (supporting information, Fig. S1). In addition to the equilibrium contact angle θ_∞ , surface tension γ and viscosity η being identical for the PS droplets on OTS and DTS in Fig. 1, the initial geometries were similar. The slip lengths, b , however, differ by an order of magnitude on these two substrates.

To investigate the droplet-dewetting process

from a modelling standpoint, we use a standard numerical implementation of the boundary element method [56, 57], allowing to integrate the axisymmetric, incompressible Stokes equation describing the flow: $\nabla P = \eta \nabla^2 \mathbf{u}$, where P is the scalar pressure field and \mathbf{u} is the velocity field. Gravity and explicit van der Waals disjoining pressure are neglected. Invoking Laplace’s equation, we further assume that the balance of normal stresses on the liquid-vapor interface is given by: $2\eta \partial_n u_n - P = 2\gamma \mathcal{C}$, where \mathcal{C} is the mean curvature of the liquid-vapor interface, and where ∂_n denotes the directional derivative normal to the free interface.

To account for slip, we use the linear Navier model [11]. Therein, the slip length $b = \eta/\kappa$ is defined through the balance of friction and viscous stresses at the solid-liquid boundary:

$$\kappa u_r|_{z=0} = \eta \partial_z u_r|_{z=0}, \quad (1)$$

where u_r is the liquid velocity parallel to the substrate, κ is the solid-liquid friction coefficient, and ∂_z denotes partial differentiation in the direction normal to the substrate. Finally, as a boundary condition at the contact line, we impose: $\theta(t) = -\arctan(\partial_r h)|_{r=R} = \theta_\infty$. Thus, the microscopic contact angle $\theta(t)$ is fixed at all times to the equilibrium Young-Dupré angle [34, 35]. In the following, we refer to this as the Navier-Young model (NYM). The constant angle assumption is not strictly correct, yet, with the small variation observed in the experimental evolution, it is a reasonable approximation (examples for $\theta(t)$ are shown in supporting information, Fig. S2).

In Fig. 2 we present the results of the NYM, for droplets with geometrical and physical parameters chosen to match the experimental droplets shown in Fig. 1. In the numerical integration of the NYM, length scales are normalized by the initial contact line radius $R(0) = R_0$, and time t is normalized through: $\mathcal{T} = t\gamma\eta^{-1}R_0^{-1}$, with \mathcal{T} the dimensionless time. In Fig. 2(a), the slip length is $B \equiv b/R_0 = 0.030$, while in Fig. 2(b) it is $B = 0.47$. These computed droplet evolutions reproduce the curvature inversion of Fig. 1(a) and its absence in Fig. 1(b), confirming that slip plays a major role in determining the transient shape. In Fig. 2, we also add experimental data from Fig. 1 for the specific profiles that maximize the deviation from a spherical cap. Those experimental profiles show

good quantitative agreement with the NYM profiles, with maximum deviations of $\sim 5\%$ of the distance from the origin. Comparison with other experiments for different droplets sizes, as well as for different times of the droplets presented in Fig. 2, show similar agreement. Finally, identifying the numerical droplet of Fig. 2(a) with the experimental one on OTS of Fig. 1(b), we note that $B = 0.03$ corresponds to a slip length $b_{\text{OTS}} = 160$ nm, that is exactly the value measured in the hole-growth dewetting experiment [29], as given above. For the droplet of Fig. 2(b) and Fig. 1(c), $B = 0.47$ corresponds to a slip length $b_{\text{DTS}} = 2250$ nm, that is similar to but larger than the measured slip length $b_{\text{DTS}} = 1500 \pm 200$ nm [29]. This slightly larger value is necessary to reproduce the experimental curve with no bump.

In view of the above agreement between numerics and experiments, the difference of droplet shapes in Fig. 1 can be explained in terms of the driving and damping forces acting on the dewetting spherical caps. The liquid motion is driven by excess interfacial energies, while the damping is provided by: i) viscous dissipation in the bulk and near the contact line; ii) friction at the solid-liquid boundary, where a smaller friction coefficient κ , and thus a larger slip length $b = \eta/\kappa$, allows for a more efficient redistribution of material. Since everything else is similar between the OTS and DTS cases of Fig. 1, the transient accumulation bump on OTS of Fig. 1(b) is thus formed due to larger friction at the substrate and subsequent limited flow towards the center of the droplet. Increasing the ratio of slip length to drop size $B = b/R_0$ is expected to lead to a vanishing of this transient bump. This is indeed observed on DTS in Fig. 1(c), where the slip length b is much higher. Similarly, using different droplet sizes on OTS – but with constant $\theta_0, \theta_\infty, b$ – the curvature inversion is seen to occur for $B \lesssim 0.06$ and thus $R_0 \gtrsim 2.7 \mu\text{m}$ (supporting information, S3).

Moving onto a description of the contact line dynamics, the scaling of $R_0 - R(t)$ for the two droplets of Fig. 1 is shown in Fig. 3(a). For ease of comparison, the contact line radius change is normalized by the total change throughout the droplet equilibration, $R_0 - R_\infty$, with R_∞ being the equilibrium contact line radius. In both OTS and DTS cases, the earliest experimentally accessible time regime shows a power-law dependence. In addition,

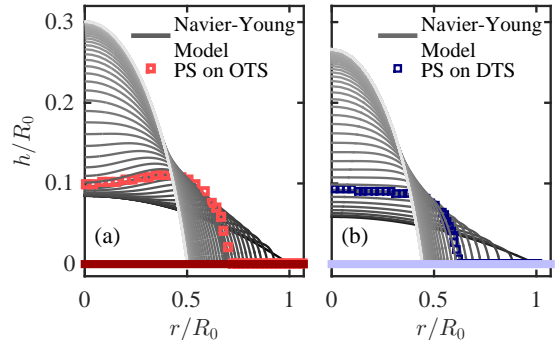


Figure 2: (a) Normalized height profile as a function of normalized radius, for different dimensionless times \mathcal{T} , for a numerical droplet evolution described by the Navier-Young model (NYM), with: $0 \leq \mathcal{T} \leq 14.5$, $B = 0.030$, $\theta_0 = 11^\circ$ and $\theta_\infty = 62^\circ$, as for the PS droplet evolution on OTS in Fig. 1(b). (b) A similar NYM droplet evolution with: $0 \leq \mathcal{T} \leq 5.2$, $B = 0.47$, $\theta_0 = 7.0^\circ$ and $\theta_\infty = 62^\circ$, as for the PS droplet on DTS in Fig. 1(c). Experimental data from the highlighted transient profiles from Fig. 1 (grey lines therein) are shown as squares.

the early-time exponents of ten other PS droplets are shown in the inset of Fig. 3(a) as a function of $b\Omega^{-1/3}$, where Ω is the droplet volume. The observed value of the dewetting exponent, m , is well represented by the average $\langle m \rangle = 0.48 \pm 0.08$, with the error representing the standard deviation. Fig. 3(b) shows the numerical NYM-evolution of the normalized contact line radius as a function of dimensionless time, for a variety of dimensionless slip lengths B . A power-law scaling similar to experiments is obtained for intermediate values, $0.03 \lesssim B \lesssim 1$, while the $B = 0.005$ and $B \geq 10$ extremes show more pronounced curvatures.

In the numerical results of the NYM for both droplets represented in Fig. 2, we observe that the early-time flow and friction are concentrated near the contact line (supporting information, Fig. S4). At early times, we thus assume the capillary driving power to be significantly dissipated by friction in the contact line region. Since the spreading parameter reads $S = \gamma(\cos\theta_\infty - 1)$, the typical driving power along the contact line is $\sim SR_0\dot{R} \sim -\gamma R_0\dot{R}$. On the other hand, since the friction stress

scales as $\sim \kappa \dot{R}$, the frictional dissipation power is $\sim \eta \dot{R}^2 R_0 \Delta / b$, where $\Delta(t)$ is the typical horizontal extension of the flow region where slip dissipation is dominant. Supported by the experimentally measured profiles near the contact line, we impose a proportionality between the vertical and horizontal extensions of the slip region. Conservation of volume thus implies a scaling $R_0 \Delta^2 \sim R_0 (R_0 - R)^2$. Balancing the capillary driving power and the slip dissipation thus leads to $\dot{R}(R - R_0) \sim \gamma b / \eta$, which can be integrated into:

$$R_0 - R(t) \sim \left(\frac{\gamma b t}{\eta} \right)^{1/2}, \quad (2)$$

consistent with the values of m reported above in both experiments and numerics. Note that this exponent and derivation are reminiscent of the slippery 2D wetting case described in Ref. [58].

The scaling argument provided above assumes that friction at the substrate is a dominant dissipation mechanism, in addition to viscous processes [47]. Using the NYM, we determine that friction at the substrate accounts for $\sim 60\%$ of the overall energy dissipation for $B = 0.030$ (OTS), and $\sim 40\%$ for $B = 0.47$ (DTS). While these are not necessarily dominating, it is clear that the relative importance of friction is the largest near the contact line. In contrast to the partial-slip scaling law derived above and in Ref. [58], no-slip hole-growth dewetting is known to show a linear power-law in time [23] (with logarithmic corrections). Similarly, following the geometrical arguments preceding Eq. 2, but with the friction replaced by viscous shear dissipation appropriate to the no-slip case, a linear power law, $R_0 - R(t) \sim t$, would be expected for dewetting droplets. The no-slip prediction falls well outside the experimentally observed range of exponents in Fig. 3, which leads us to suggest that dissipation *in the contact line region* is dominated by slip friction in our system.

Finally, we examine the late-time contact line dynamics. Figs. 4(a) and (b) show the rescaled-normalized contact line radius as a function of time for dewetting-microdroplet experiments on OTS and DTS covered substrates. Fig. 4(c) shows the results obtained from the NYM for various B . As expected for an approach to equilibrium, in all cases an exponential evolution is reached as the contact line radius approaches the equilibrium value

R_∞ . Furthermore, on DTS, and for the smallest droplets on OTS, and at large B in the NYM, the droplets reach the exponential regime at much larger $R - R_\infty$. Interestingly, an exponential evolution is also characteristic of suspended relaxing viscous droplets that have been deformed by a shear flow [59,60]. Thus, a connection can be drawn between supported droplets with large slip lengths and free-standing droplets. In fact, by symmetry, the freely relaxing droplets are strictly equivalent to full-slip dewetting droplets when $\theta_\infty = 90^\circ$.

The late-time exponential evolution can be understood from scaling arguments. Near equilibrium, the droplet shape is nearly a spherical cap,

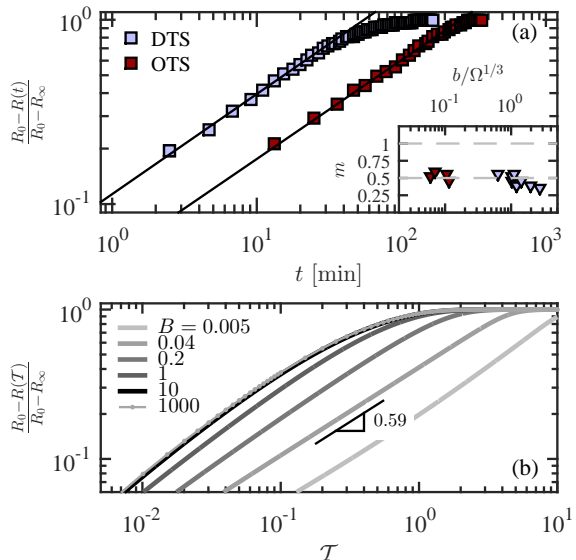


Figure 3: (a) Experimental early-time dynamics of the rescaled contact line radius, for the two PS droplets of Fig. 1 dewetting from OTS and DTS substrates. Solid lines represent power laws t^m , with exponent $m = 0.54$. The inset shows such exponents measured for all studied droplets for which an early-time dynamics was accessible, as a function of $b\Omega^{-1/3}$ where Ω is the droplet volume; the dashed lines indicate $m = 0.5$ and $m = 1$. (b) Numerical early-time dynamics obtained from the NYM using various $B = b/R_0$. Along with unit initial radius, parameters used were $\theta_0 = 9.9^\circ$, $\theta_\infty = 62^\circ$, leading to $R_\infty/R_0 \approx 0.54$.

and the restoring capillary force is linear in $R - R_\infty$ (supporting information, Eq. S13). Therefore, the driving power scales as $\mathcal{P}_{\text{inj}} \sim -\gamma(R - R_\infty)\dot{R}$. On the other hand, three possible dissipation mechanisms can be at play in the system: i) friction at the substrate, ii) viscous shear flow, and iii) viscous elongational flow. As a consequence, the dissipation power \mathcal{P}_{dis} is generally expected to depend on exactly four parameters: η , b , θ_∞ , R_∞ , and one variable: the contact line velocity \dot{R} . According to the Π -theorem [61], and since θ_∞ is constant in this study, we are left with two independent dimensionless groups. Therefore, the dissipation power is necessarily of the form: $\mathcal{P}_{\text{dis}} \sim \eta R_\infty \dot{R}^2$, with a dimensionless prefactor that is a function of b/R_∞ and θ_∞ . Balancing the dissipation power with the driving one, and integrating in time leads to:

$$R(t) - R_\infty \sim e^{-t/\tau}, \quad (3)$$

$$\tau = \frac{\eta R_\infty}{\gamma} f\left(\frac{b}{R_\infty}, \theta_\infty\right), \quad (4)$$

where f absorbs all the missing numerical prefactors associated with the scaling arguments presented above, as well as the geometrical dependence, *i.e.* θ_∞ . In Fig. 4(d), we plot the time constant τ of the late-time exponential behaviors in Figs. 4(a) and (b), as a function of the dimensionless slip length b/R_∞ , using the slip lengths measured in the present study: $b_{\text{OTS}} = 160$ nm and $b_{\text{DTS}} = 2250$ nm. Also shown are the late-time exponential time constants obtained from various realizations of the NYM shown in Fig. 4(c). The numerical results allow for an estimation of the function f .

When $b/R_\infty \ll 1$, we are in the framework of the classical wedge-calculation [21, 33], where the slip length b replaces the smaller microscopic cut-off length scale in a logarithmic prefactor. In this limit, it follows (supporting information) for a spherical cap in the small-angle approximation: $f = C_0 \ln(b/R_\infty) + C_1$. We find $C_0 \approx -1.44$ for $\theta_\infty = 62^\circ$. In the weak-slip regime of Fig. 4(d), the logarithmic dependence is indeed observed in the NYM. There we see $C_0^{\text{NYM}} = -1.02$ and an offset $C_1^{\text{NYM}} = -0.65$, obtained by fitting the $B \leq 0.08$ NYM data. This is in reasonable agreement with the prediction quoted above and detailed in the supplemental material.

In contrast, when $b/R_\infty \gg 1$, the localized con-

tact line dissipation assumption of the wedge approach is violated. Friction at the substrate is negligible with respect to elongational viscous stresses,

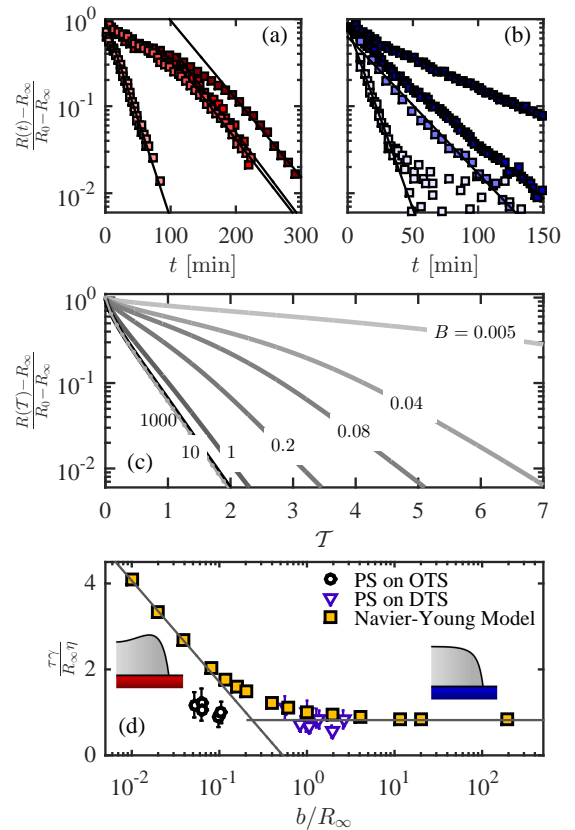


Figure 4: Late-time dynamics of normalized contact line radius for three cases: (a) PS droplets dewetting from OTS substrates with $2.7 \leq R_0 \leq 5.3 \mu\text{m}$; (b) PS droplets dewetting from DTS substrates $1.8 \leq R_0 \leq 7.7 \mu\text{m}$; (c) numerical results from the NYM, with dimensionless slip lengths B as indicated on the curves. (d) Dimensionless relaxation time-constant as a function of the dimensionless slip length, for both the experiments and the NYM. The two lines depict the asymptotic behaviours (see text): i) partial-slip logarithmic behaviour; ii) strong-slip constant behaviour ($B = 1000$ not shown). The insets schematically show intermediate-time droplet shapes, representative of the weak slip (red substrate) and strong slip (blue substrate) regimes.

and a different retraction regime is entered. In this regime, we expect f to be independent of b/R_∞ . We find $f|_{b \rightarrow \infty} \approx 0.82$ for $\theta_\infty = 62^\circ$ in the NYM; the experiments on DTS support this finding. The NYM value for the large slip relaxation time compares well with an argument, based on purely elongational viscous stresses, predicting that $f|_{b \rightarrow \infty} \approx 1.05$ for $\theta_\infty = 62^\circ$ (see supporting information).

The numerical model and scaling approach, with Navier slip and Young-angle boundary condition, have corroborated the experimental height-profile evolutions, and have reproduced the main features of the contact line dynamics. However, we caution that the agreement is not quantitative in all respects. At small b/R_∞ , the experimental time constants in Fig. 4(d) deviate from the NYM data and the scaling asymptotics. Several effects may explain this discrepancy: non-linear [46] or spatially non-uniform [47, 48] slip may be operative; the assumption of constant microscopic contact angle [34, 35], $\theta(t) = \theta_\infty$, could be relaxed as well (see supporting information); furthermore, in ultra-thin (~ 5 nm) dewetting polymer films, thermal fluctuations are known to enhance the dynamics [62], which could also affect the effective liquid mobility at the solid-liquid boundary, or at the three-phase contact line. Additionally, at relatively small slip length, other mechanisms of CLM may contribute [33]. The present results thus open a perspective to more detailed studies from both theoretical and experimental sides.

To conclude, we have studied polymer microdroplets dewetting from substrates decorated with self-assembled monolayers (SAMs), where the initial contact angle much smaller than the equilibrium one. The OTS SAM provides a weaker slip boundary condition as compared to the DTS, resulting in marked differences in the evolution of similarly-sized droplets. Specifically, the weaker slip condition can give rise to transient non-convex interfacial shapes. Increasing the ratio of slip length to droplet size, we observe a smooth transition to purely convex shapes. At early times, we find that the early time dewetting kinetics in our experiments is consistent with a scaling argument predicting a temporal power-law evolution of the contact line radius, with an exponent $m = 1/2$. In addition, numerical integration of the Navier-Young model leads to $m \approx 0.59$ for intermediate

slip lengths. At late times, or when the slip length is large compared to the droplet size, an exponential relaxation of the contact line radius with time is observed, as for the relaxation of a freely suspended ellipsoidal droplet. Once again, the behaviour and time constants are in good agreement with scaling analysis and numerical resolution of the Navier-Young model. The simple geometry of relaxing droplets gives insight onto the effect of slip in free surface nano- and micro-flows. An increase in the slip length leads to a more uniform flow field throughout the droplet, and a spreading of the dissipation throughout the bulk. The dispersion of dissipation is evidenced using visualizations of the NYM slip friction. Furthermore, the experimental observation also confirmed by the NYM model, of bump formation for relatively small slip lengths, and a lack thereof for relatively large slip lengths illustrates a change in the dominant dissipation mechanism. In the context of the Huh-Scriven paradox of contact line motion (suggesting that contact lines require infinite energy to be put in motion), our work offers a combined experimental and theoretical justification for slip as a major contributor to divergence relief; however, the low slip experimental data suggests that other forces may need to be considered when slip is weak.

Materials and Methods

To prepare the non-equilibrium droplets, PS (Polymer Standards Service GmbH, Mainz, Germany) with weight-averaged molecular weight 10.3 kg/mol, and polydispersity index 1.03, was dissolved into toluene (chromatography grade, Merck, Darmstadt, Germany), and spin-coated onto freshly cleaved mica sheets (grade V2; Plano GmbH, Wetzlar, Germany). After a dewetting process in toluene-saturated atmosphere at room temperature, glassy spherical cap shaped droplets on mica were produced with initial contact angles $\theta_0 = 9 \pm 3^\circ$, and contact line radii $2 \mu\text{m} \lesssim R_0 \lesssim 7 \mu\text{m}$ (measured using AFM; Dimension FastScan and FastScan A tips, Bruker, Karlsruhe, Germany).

Under ambient conditions, the glassy droplets were then floated from the mica onto the surface of an ultraclean water bath (18 M Ω cm, total organic carbon content < 6 ppb; TKA-GenPure, TKA Wasseraufbereitungssysteme GmbH, Niederelbert, Germany), and transferred onto the SAM-coated silicon wafers ((100) crystal orientation with na-

tive oxide layer present; Si-Mat Silicon Materials, Kaufering, Germany). Two types of SAMs were used, being prepared from either octadecyltrichlorosilane or dodecyltrichlorosilane molecules (OTS or DTS; Sigma-Aldrich, Munich, Germany), with the self-assembly procedure and full characterization described in Ref. [63]. Both SAM coatings render the Si wafers hydrophobic, and lead to equilibrium PS contact angles in air of $\theta_\infty = 62 \pm 3^\circ$, as measured by AFM. The use of OTS and DTS substrates is thus particularly advantageous in this study, as they present different slip lengths for PS, but have the same θ_∞ with PS in air [29, 55].

Since the initial contact angle θ_0 of the glassy droplets is much smaller than the equilibrium angle θ_∞ , they are susceptible to dewetting when heated above the glass-transition temperature, $T_g \approx 90^\circ\text{C}$ [64]. The built-in heating stage on the AFM was thus set to $T = 110^\circ\text{C}$, and AFM was used to measure *in situ* height profiles of the dewetting polymer microdroplets. This annealing temperature is also low enough to ensure no loss of PS due to evaporation or degradation, and volume conservation was verified. Finally, the capillary velocity of our system was measured using the stepped-film method [65] to be $\gamma/\eta = 0.07 \pm 0.01 \mu\text{m s}^{-1}$ at the experimental annealing temperature.

Acknowledgments

The authors gratefully acknowledge NSERC of Canada, the Alexander von Humboldt Foundation, the German Science Foundation, BP and Total for financial support.

References

- [1] L. Bocquet and E. Charlaix. Nanofluidics, from bulk to interfaces. *Chemical Society Reviews*, 39:1073, 2009.
- [2] C. Neto, D.R. Evans, E. Bonaccorso, H.-J. Butt, and V.S.J. Craig. Boundary slip in newtonian liquids: a review of experimental studies. *Reports on Progress in Physics*, 68:2859, 2005.
- [3] E. Lauga, M.P. Brenner, and H.A. Stone. *Handbook of Experimental Fluid Mechanics*, chapter 19: Microfluidics : The No-Slip Boundary Condition. Springer, New York, 2007.
- [4] K. Falk, F. Sedlmeier, L. Joly, R.R. Netz, and L. Bocquet. Molecular origin of fast water transport in carbon nanotube membranes: superlubricity versus curvature dependent friction. *Nano Letters*, 10:4067, 2010.
- [5] M. Whitby, L. Cagnon, M. Thanou, and N. Quirke. Enhanced fluid flow through nanoscale carbon pipes. *Nano Letters*, 8:2632, 2008.
- [6] A. Cuenca and H. Bodiguel. Submicron flow of polymer solutions: Slippage reduction due to confinement. *Physical Review Letters*, 110:108304, 2013.
- [7] S.A. Setu, R.P.A. Dullens, A. Hernández-Machado, I. Pagonabarraga, D.G.A.L. Aarts, and R. Ledesma-Aguilar. Superconfinement tailors fluid flow at microscales. *Nature Communications*, DOI: 10.1038/ncomms8297, 2015.
- [8] O. Bäümchen, L. Marquant, R. Blossey, A. Münch, B. Wagner, and K. Jacobs. Influence of slip on the rayleigh-plateau rim instability in dewetting viscous films. *Physical Review Letters*, 113:014501, 2014.
- [9] O. Bäümchen, R. Fetzer, and K. Jacobs. Reduced interfacial entanglement density affects the boundary conditions of polymer flow. *Physical Review Letters*, 103:247801, 2009.
- [10] Sabrina Haefner, Michael Benzaquen, Oliver Bäümchen, Thomas Salez, Robert Peters, Joshua D. McGraw, Karin Jacobs, Élie Raphaël, and Kari Dalnoki-Veress. Influence of Slip on the Plateau-Rayleigh Instability on a Fibre. *Nature Communications*, 6:7409, 2015.
- [11] CMLH Navier. Mémoire sur les lois du mouvement des fluides. *Mem. Acad. Sci. Inst. Fr.*, 6:389, 1823.
- [12] J.-H. J. Cho, B.M. Law, and F. Rietaud. Dipole-dependent slip of newtonian liquids at smooth solid hydrophobic surfaces. *Physical Review Letters*, 92:166102, 2004.

- [13] L. Joly, C. Ybert, and L. Bocquet. Probing the nanohydrodynamics at liquid-solid interfaces using thermal motion. *Physical Review Letters*, 96:046101, 2006.
- [14] C. Cottin-Bizonne, A. Steinberger, B. Cross, O. Raccurt, and E. Charlaix. Nanohydrodynamics : The intrinsic flow boundary condition on smooth surfaces. *Langmuir*, 24:1165, 2008.
- [15] S. Guriyanova, B. Semin, T. S. Rodrigues, H. J. Butt, and E. Bonaccorso. Hydrodynamic drainage force in a highly confined geometry: Role of surface roughness on different length scales. *Microfluid Nanofluid*, 8:653, 2010.
- [16] A. Maali and B. Bhushan. Slip-length measurement of confined air flow using dynamic atomic force microscopy. *Phys. Rev. E*, 78:027302, 2008.
- [17] C. Lissandrello, V. Yakhot, and K.L. Ekinci. Crossover from hydrodynamics to the kinetic regime in confined nanoflow. *Physical Review Letters*, 108:084501, 2012.
- [18] R. Pit, J. Hervet, and L. Léger. Direct experimental evidence of slip in hexadecane: Solid interfaces. *Physical Review Letters*, 85:980, 2000.
- [19] T. Schmatko, H. Hervet, and L. Leger. Friction and slip at simple fluid-solid interfaces: The roles of the molecular shape and the solid-liquid interaction. *Physical Review Letters*, 94:244501, 2005.
- [20] S. Leroy, F. Restagno, and E. Charlaix. Fine calibration of the residual dissipation in a surface forces apparatus using a capacitive sensor. *Review of Scientific Instruments*, 80:085103, 2009.
- [21] P.G. de Gennes. Wetting: Statics and Dynamics. *Reviews of Modern Physics*, 57:827, 1985.
- [22] P.G. de Gennes. *Soft Interfaces: The 1994 Dirac Memorial Lecture*. Cambridge University Press, 1997.
- [23] F. Brochard-Wyart, P.G. de Gennes, H. Hervet, and C. Redon. Wetting and slippage of polymer melts on semi-ideal surfaces. *Langmuir*, 10:1566, 1994.
- [24] J. Galt and B. Maxwell. Velocity profiles for polyethylene melts. *Modern Plastics*, December 1964.
- [25] G. Reiter and R. Khanna. Kinetics of auto-phobic dewetting of polymer films. *Langmuir*, 16:6351, 2000.
- [26] L. Leger. Friction mechanisms and interfacial slip at fluid – solid interfaces. *Journal of Physics: Condensed Matter*, 15:S19, 2003.
- [27] R. Fetzer, K. Jacobs, A. Münch, B. Wagner, and T.P. Witelski. New slip regimes and the shape of dewetting thin liquid films. *Physical Review Letters*, 95:127801, 2005.
- [28] R. Fetzer, A. Münch, B. Wagner, M. Rauscher, and K. Jacobs. Quantifying hydrodynamic slip: A comprehensive analysis of dewetting profiles. *Langmuir*, 23:10559, 2007.
- [29] J.D. McGraw, O. Bäümchen, M. Klos, S. Haefner, M. Lessel, S. Backes, and K. Jacobs. Nanofluidics of thin polymer films: Linking the slip boundary condition at solid-liquid interfaces to macroscopic pattern formation and microscopic interfacial properties. *Journal of Colloid and Interface Science*, 210:13, 2014.
- [30] C. Huh and L.E. Scriven. Hydrodynamic model of steady movement of a solid/liquid/fluid contact line. *Journal of Colloid and Interface Science*, 35:85, 1971.
- [31] P.G. de Gennes, F. Brochard-Wyart, and D. Quéré. *Capillarity and Wetting Phenomena: Drops, Bubbles, Pearls, Waves*. Springer, New York, 2003.
- [32] T. Blake. The physics of moving wetting lines. *Journal of Colloid and Interface Science*, 299:1, 2006.
- [33] D. Bonn, J. Eggers, J. Indekeu, J. Meunier, and E. Rolley. Wetting and spreading. *Reviews of Modern Physics*, 81:739, 2009.

- [34] J.H. Snoeijer and B. Andreotti. Moving contact lines: Scales, regimes, and dynamical transitions. *Annual Review of Fluid Mechanics*, 45:269, 2013.
- [35] D.N. Sibley, A. Nold, N. Savva, and S. Kalliadasis. A comparison of slip, disjoining pressure, and interface formation models for contact line motion through asymptotic analysis of thin two-dimensional droplet spreading. *Journal of Engineering Mathematics*, DOI: 10.1007/s10665-014-9702-9, 2014.
- [36] E.B. Dussan V. and S.H. Davis. On the motion of a fluid-fluid interface along a solid surface. *Journal of Fluid Mechanics*, 65:71, 1974.
- [37] P.C. Wayner. Spreading of a liquid film with a finite contact angle by the evaporation/condensation process. *Langmuir*, 9:294, 1993.
- [38] K. Davitt, M.S. Pettersen, and E. Rolley. Thermally activated wetting dynamics in the presence of surface roughness. *Langmuir*, 29:6884, 2013.
- [39] F. Heslot, A.M. Cazabat, and N. Fraysse. Diffusion-controlled wetting films. *Journal of Physics: Condensed Matter*, 1:5793, 1989.
- [40] A.M. Cazabat, S. Gerdes, M.P. Valignat, and S. Vilette. Dynamics of wetting: From theory to experiment. *Interface Science*, 5:127, 1997.
- [41] H.P. Kavehpour, B. Ovrzyn, and G.H. McKinley. Microscopic and macroscopic structure of the precursor layer in spreading viscous drops. *Physical Review Letters*, 91:196104, 2003.
- [42] M. Ghosh and K.J. Stebe. Spreading and retraction as a function of drop size. *Advances in Colloid and Interface Science*, 161:61, 2010.
- [43] A. Hoang and H. P. Kavehpour. Dynamics of nanoscale precursor film near a moving contact line of spreading drops. *Physical Review Letters*, 106:254501, 2011.
- [44] S. Cormier, J. McGraw, T. Salez, É. Raphaël, and K. Dalnoki-Veress. Beyond tanner’s law: Crossover between spreading regimes of a viscous droplet on an identical film. *Physical Review Letters*, 109:154501, 2012.
- [45] I. Cantat. Liquid meniscus friction on a wet plate : Bubbles , lamellae , and foams. *Physics of Fluids*, 25:031303, 2014.
- [46] P.A. Thomson and S.M. Troian. A general boundary condition for liquid flow at solid surfaces. *Science*, 389:360, 1997.
- [47] H. B. van Lengerich and P. H. Steen. Energy dissipation and the contact-line region of a spreading bridge. *Journal of Fluid Mechanics*, 703:111, 2012.
- [48] E. Kirkinis and S. H. Davis. Hydrodynamic theory of liquid slippage on a solid substrate near a moving contact line. *Physical Review Letters*, 110:234503, 2013.
- [49] R. Weiqing and E. Weinan. Boundary conditions for the moving contact line problem. *Physics of Fluids*, 19:022101, 2007.
- [50] J. Marsh, S. Garoff, and E. Dussan V. Dynamic contact angles and hydrodynamics near a moving contact line. *Physical Review Letters*, 70:2778, 1993.
- [51] G. Delon, M. Fermigier, J. H. Snoeijer, and B. Andreotti. Relaxation of a dewetting contact line part 2: Experiments. *Journal of Fluid Mechanics*, 604:55, 2008.
- [52] E. Elizalde, R. Urteaga, R.R. Koropeccki, and C.L.A. Berli. Inverse problem of capillary filling. *Physical Review Letters*, 112:134502, 2014.
- [53] J. Eggers. Existence of receding and advancing contact lines. *Journal of Fluid Mechanics*, 17:082106, 2005.
- [54] T.S. Chan, T. Gueudré, and J.H. Snoeijer. Maximum speed of dewetting on a fiber. *Physics of Fluids*, 23:112103, 2011.
- [55] O. Bäümchen, R. Fetzer, M. Klos, M. Lessel, L. Marquant, H. Hähl, and K. Jacobs. Slippage and nanorheology of thin liquid polymer films. *Journal of Physics: Condensed Matter*, 24:325102, 2012.
- [56] C. Pozrikidis. Interfacial dynamics for stokes flow. *Journal of Computational Physics*, 169:250, 2001.

- [57] C. Pozrikidis. *A Practical Guide to Boundary Element Methods*. Chapman & Hall/CRC, 2002.
- [58] Y. Nakamura, A. Carlson, G. Amberg, and J. Shiomi. Dynamic wetting at the nanoscale. *Physical Review E*, 88:033010, 2013.
- [59] J. Rallison. The deformation of small viscous drops and bubbles in shear flows. *Annual Review of Fluid Mechanics*, 16:45, 1984.
- [60] S. Guido and M. Villone. Measurement of interfacial tension by drop retraction analysis. *Journal of Colloid and Interface Science*, 209:247, 1999.
- [61] G.I. Barenblatt. *Scaling*. Cambridge University Press, 2003.
- [62] R. Fetzer, M. Rauscher, R. Seemann, K. Jacobs, and K. Mecke. Thermal noise influences fluid flow in thin films during spinodal dewetting. *Physical Review Letters*, 99:114503, 2007.
- [63] M. Lessel, O. Bäumchen, M. Klos, H. Hähl, R. Fetzer, R. Seemann, M. Paulus, and K. Jacobs. Self-assembled silane monolayers: An efficient step-by-step recipe for high-quality, low energy surfaces monolayers: an efficient step-by-step recipe for high-quality, low energy surfaces. *Surface and Interface Analysis*, 47:557, 2015.
- [64] P.G. Santangelo and C.M. Roland. Molecular weight dependence of fragility in polystyrene. *Macromolecules*, 31:4581, 1998.
- [65] J.D. McGraw, T. Salez, O. Bäumchen, E. Raphaël, and K. Dalnoki-Veress. Self-similarity and energy dissipation in stepped polymer films. *Physical Review Letters*, 109:128303, 2012.